AD NUMBER

AD245163

LIMITATION CHANGES

TO:

Approved for public release; distribution is unlimited.

FROM:

Distribution authorized to U.S. Gov't. agencies only; Administrative/Operational Use; 26 JUL 1960. Other requests shall be referred to Office of Naval Research, One Liberty Center, 875 North Randolph Street, Arlington, VA 22203-1995.

AUTHORITY

ONR ltr dtd 9 Nov 1977

DISCLAIMER NOTICE

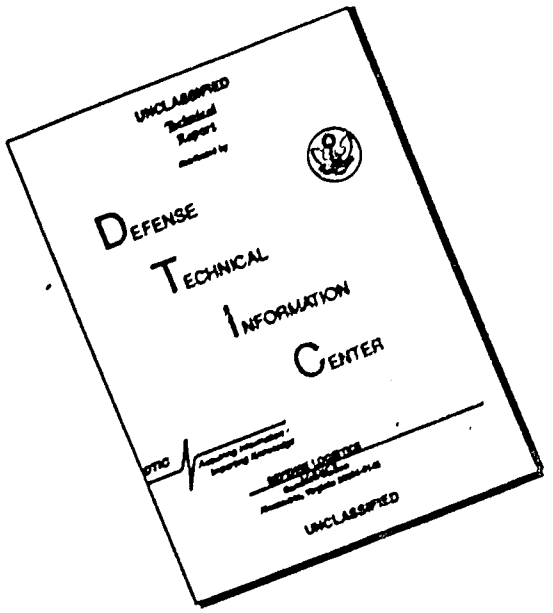

THIS DOCUMENT IS BEST QUALITY AVAILABLE. THE COPY FURNISHED TO DTIC CONTAINED A SIGNIFICANT NUMBER OF PAGES WHICH DO NOT REPRODUCE LEGIBLY.

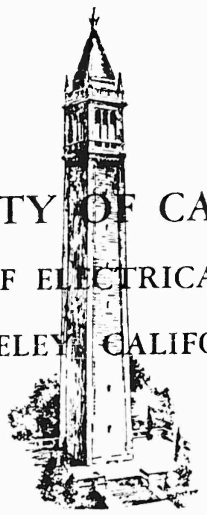

UNIVERSITY OF CALIFORNIA
DEPARTMENT OF ELECTRICAL ENGINEERING
BERKELEY, CALIFORNIA

ELECTRONICS RESEARCH LABORATORY

BACK-SCATTERING FROM DIELECTRIC CONES

by

C. Y. Pon
D. J. Angelakos

Institute of Engineering Research
Series No. 60, Issue No. 300
July 26, 1960
Nonr-222(74)

Electronics Research Laboratory
Department of Electrical Engineering
University of California
Berkeley, California

Series No. 60
Issue No. 330

BACK-SCATTERING FROM DIELECTRIC CONES

by

C. Y. Pon
D. J. Angelakos

Report No. 110
Office of Naval Research
Contract Nonr-222(74)

July 26, 1960

ABSTRACT

The boundary value problem of scattering by objects may be solved by exact electromagnetic theory, approximate methods, or experimental measurements, depending on the complexity of shape and the characteristic dimension of the body. So far the number of experimental investigations is relatively few compared to the number of theoretical treatments. The principal objective of this research was to measure the back-scatter cross sections of a family of right circular dielectric cones of finite dimensions. A highly accurate image plane method was used for the measurements. The results indicate that considerable difference exists between the metal cones and dielectric cones, even for dielectric constants up to 20. The back-scatter patterns show more lobes for the dielectric cones than for the metal cones. A surprisingly large reflection from the larger size dielectric cones was observed for the nose-on aspect where it was practically unobservable for the metal cones. In some cases, the reflections for the nose-on aspect exceeded the reflections for the base-on aspect.

TABLE OF CONTENTS

LIST OF FIGURES

LIST OF TABLES

I. INTRODUCTION

Now considerable attention is focused on the scattering characteristics of various forms of bodies relevant to practical objects such as future space vehicles which have gained tremendously in development. It is desirable to determine, as accurate as possible for as many different shapes as practicable, their scattering characteristics from which one can apply them in connection with the problems of detection, tracking, and guidance. It is obvious that the study of "diffraction and scattering," which formerly attracted primarily academic interest, is now considered to be significant for practical as well as academic reasons.

Any object placed in the path of an incident electromagnetic wave will have currents induced in it which, in turn, radiate a new wave defined as the scattered wave. The electric field excited by this induced source combines vectorially with the incident electric field to give a total electric field, which is defined as the diffracted field. Hence, a knowledge of any two of the three field vectors is sufficient to solve the scattering problem, since one field vector is either the vector sum or difference of the other two field vectors.

Several methods, both exact and approximate, had been developed for solving the scattering problems. The relative advantage of each method depends on the problem at hand. For instance, scattering by objects with simple geometry such as a sphere may be solved exactly by the classical methods. Many well-known techniques in the field of optics greatly facilitate the determination of scattering by objects large compared with the wavelength of the incident wave. On the other hand, the most convenient method of finding the field scattered by complex shape objects comparable to a wavelength is that of experimental measurements.

In most practical cases, theoretical treatment of scattering by finite size bodies is extremely complicated. Most analytical methods consist of a series of approximations that lean heavily on the laws of sound or optics, depending on the characteristic dimension

of the scatterer. When the characteristic dimension of the body is small comparing with the wavelength, Rayleigh's laws pertaining to scattering of sound waves are applicable. When the characteristic dimension of the body is large compared with the wavelength, the methods of physical optics may be employed. As the wavelength becomes vanishingly small with respect to the size of the scatterer, the methods of geometric optics or ray optics are applicable. K. M. Siegel has discussed these methods extensively and has found excellent agreement between the results obtained by physical optics, exact electromagnetic theory, and experiment for an infinite conducting cone.[1] Also, theoretical treatments dealing with a class of simple perfectly conducting scatterers are given by Crispin, Jr., Goodrich, and Siegel in a recent report. For purpose of comparison, the ratio of the radar cross section of a dielectric object to that of a perfectly conducting object is given as:[2]

In the geometric region: $$\frac{\sigma_{diel}}{\sigma_{p.\,cond}} = \left(\frac{\sqrt{\epsilon_r}-1}{\sqrt{\epsilon_r}+1}\right)^2$$

In the Rayleigh Region: (sphere result) $$\frac{\sigma_{diel}}{\sigma_{p.\,cond}} = \frac{4}{9}\left|\frac{\epsilon_r-1}{\epsilon_r+2}\right|^2$$

$$\epsilon_r \gg 1$$

Since the sizes of the cones used in this research are in neither of these two regions, the above formulas are not strictly applicable here. However, comparing the values calculated from these formulas with the values obtained from experimental measurements on the cones and knowing the degree of accuracy desired, one can determine whether the application of these methods to solve the scattering problem is justified.

II. EXPERIMENTAL MEASUREMENTS

Since a rigorous solution to the scattering problem of most practical objects is formidable, if not impossible, consequently, it is necessary to resort to the less accurate, but nevertheless reliable, method of experimental measurements, which is the principal objective of this research. The results obtained not only reveal the scattering characteristics, but also serve as a means of evaluating the validity of the approximate solutions obtained by geometric optics, physical optics, and the variational method to determine the range of applicability of these methods. Furthermore, exact solutions to objects which readily lend themselves to the formal methods, as in the case of a sphere, would ultimately have to be substantiated by measurements.

The measurements performed in this research are the backscatter cross sections, or monostatic radar cross sections, as a function of aspect angle. The objects of interest are three different sizes of cones with base diameters of 1.267 in., 1 in., and 0.619 in., and all have apex angle of 15°. Corresponding to each size of cones are four relative dielectric constants of 5, 10, 15, and 20. Further details of these cones are listed in Table 8.

A. MEASUREMENT APPARATUS

The apparatus used in this research has been built and improved by several investigators over a period of years until highly accurate results are attainable. Complete details of the instrumentations are available in a report by Honda, Silver and Clapp,[3] and in Honda's M. S. thesis.[4] The modifications made on the measuring system and the investigation of the sources of errors are described in Olte's doctorate dissertation.[5] Here a brief description of the measuring system is sufficient to aid the interpretation and estimation of accuracy of the results.

The elements shown in Fig. 1 constitute the measuring system which is known as the image plane technique. The signal from an X-band klystron oscillator, which is stabilized to a frequency deviation

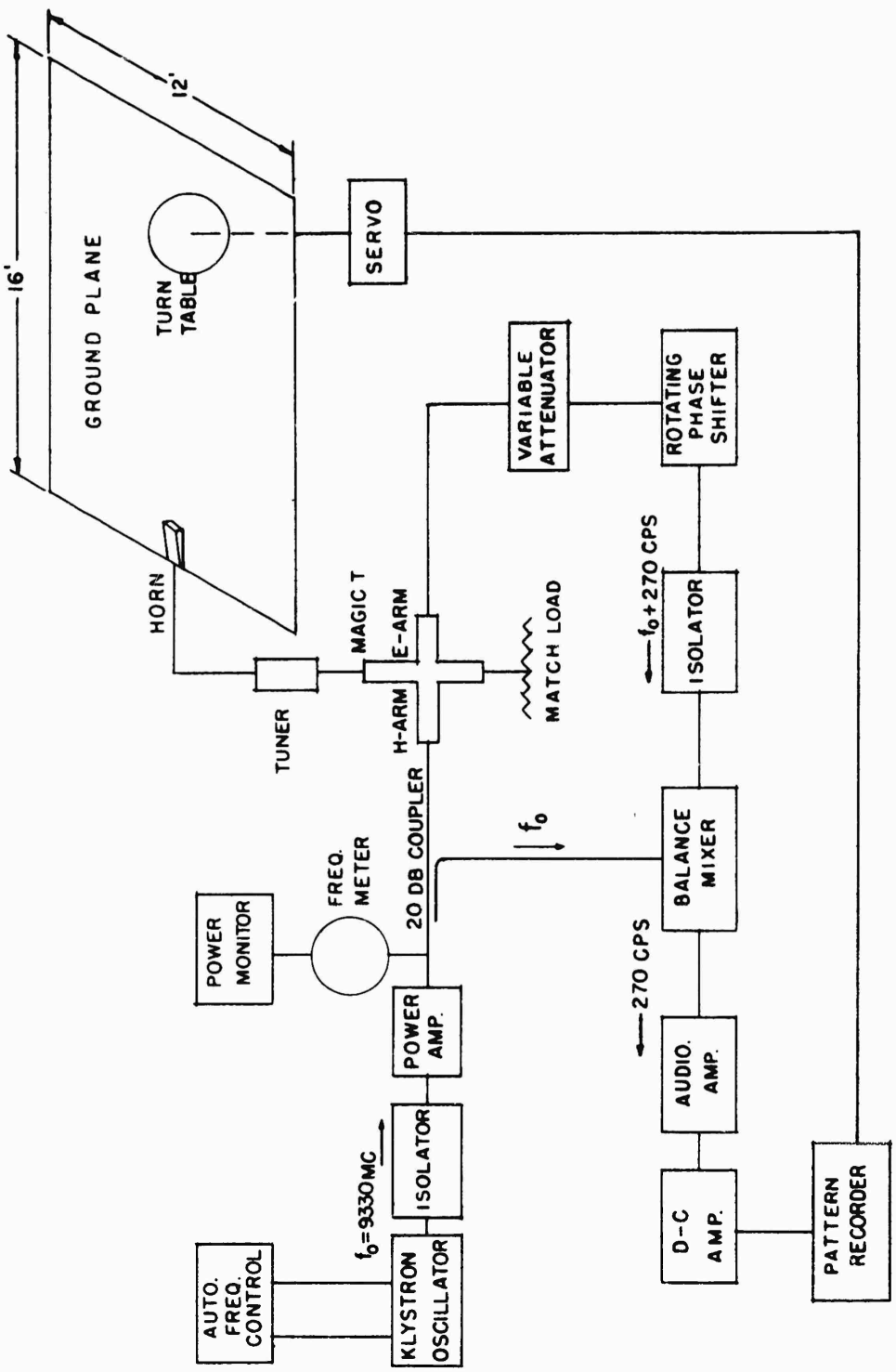

FIG.1 MEASUREMENT SYSTEM

within $\pm$ 50 kc/sec by an automatic frequency control system, is amplified to about four watts of power. This power is fed into the H-plane arm of a "magic" T and splits equally between the two side arms, one of which is terminated by a matched load and the other is connected to the horn which illuminates the ground plane. The reflected signal is received by the same horn and is detected at the E-plane arm of the "magic" T. After passing through a calibrated attenuator, the signal is phase modulated by a rotating phase shifter at 270 cps, thus changing the received signal to a frequency of f_0 + 270 cps. This signal is then combined with the reference signal of frequency f_0 in the balance mixer, giving an output signal of 270 cps, which is amplified by an audio amplifier. Finally, the output from the audio amplifier is rectified and then amplified by a d-c amplifier which drives a recorder.

The turntable on the ground plane upon which the targets are to be placed may be rotated manually. The rotations of the pattern recorder and the turntable are synchronized by a servo system. Obviously, this image plane technique is suitable for measurements of objects which are figures of revolutions only.

B. SOURCES OF ERRORS

Theoretically, accurate results are obtained when, without the target on the ground plane, the power flowing out the two side arms of the "magic" T are equal. In other words, the "magic" T, which is essentially a bridge circuit, is perfectly balanced by a set of tuning screws on the side arm feeding the horn, cancelling all the extraneous reflections from surrounding obstacles so that the only signal detected is from the target. Despite numerous efforts exerted into increasing the precision and accuracy of the system, certain imperfections evolving from the physical environment are unavoidable.

The main source of error is the undesired reflections from the room walls and fixtures and from the edge of the ground plane. The residual signal within the "magic" T itself and the multiple scattering between the target and walls also contribute to errors in measurements. Since it is practically impossible to cancel all the undesired reflections,

consequently, the back-scattered signal from a target has a periodic variation, arising from the difference in phase between the target and background reflections, as the target is pulled away from the horn.

C. PROCEDURE

By proper adjustment of the set of tuning screws, the background reflections, in absence of the target, are tuned out as much as possible as indicated by the null reading on the meter connected to the E-plane arm. Then we place the target on the ground plane and proceed with the measurements.

For accurate measurements it is necessary to make a plot of the back-scattered field versus the distance of the target from the horn. This plot is facilitated by pulling the target along the ground plane by a motor of constant speed and simultaneously recording the back-scattered field on a chart attached to a rolling recorder of constant speed. The resulting graph displays the details of the field oscillations, with period equals to one half of a wavelength, about the mean value, which decreases with increasing distance.

The mean value of the oscillations, which may be determined graphically from the plot, at each point is taken to be the back-scattered field from the target at that particular point. By definition, the back-scatter cross section of an object is a far zone parameter; therefore, the graph also enables one to ascertain whether the target is in the far zone, a condition which is satisfied when the back-scattered field is inversely proportional to the square of the distance between the target and horn.

Since the primary interest of this research is the back-scattering from each aspect angle of the dielectric cone, showing the complete pattern over 360°, it is not feasible to use the averaging method mentioned above for every angle of the cone. Therefore, two types of measurements are to be performed, the accuracies of which shall be elaborated later.

The purpose of the first type of measurement is to obtain a pattern of the back-scattered field over 360°. The cone is placed on

the center of the turntable, with the center of the cone, which is chosen to correspond to its center of gravity, coinciding with the center of the turntable. Then the turntable is rotated slowly and the pattern is traced by the polar recorder. In view of the oscillatory behavior of the return signal described previously, one would expect the pattern obtained by this method to give a qualitative rather than a quantitative picture of the back-scatter characteristics. However, the degree of accuracy of this measurement may be estimated by the second type of measurement described in the next paragraph.

The purpose of the second type of measurement is to obtain results with better accuracy than the first method by an averaging process.[6] Since the period of oscillation is equal to one-half of a wavelength, the average of the two return signals taken a quarter of a wavelength apart will approximate the true back-scattering from the target. The spatial attenuation, which is proportional to $1/R^2$, of the back-scattered field over the quarter wavelength has been ignored because the object is about eighty wavelengths away from the horn so that the difference of the mean values at two points a short distance apart is negligible.

Unfortunately, there is no way by which the cones may be rotated mechanically at points other than the center of the turntable such that the complete pattern is recorded at the same time. Consequently, when the measurements are taken at either of the points spaced a quarter wavelength apart, it is necessary to place the cone each time at a preselected angle and to record the return signal at that angle. Since it is laborious and time consuming to carry out measurements for a large number of aspect angles by this method because of the height and size of the ground plane, only the prominent features, which consist of the base, tip, and major lobes, of each pattern shall be measured by this method.

For this image plane technique, the incident electric field is perpendicular to the ground plane as shown in Fig. 2. The cones are measured at the far zone, and the back-scatter cross section for any aspect angle is defined as

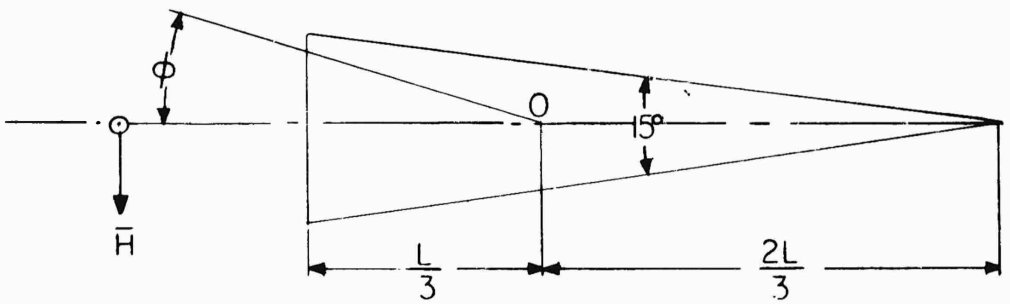

TOP VIEW

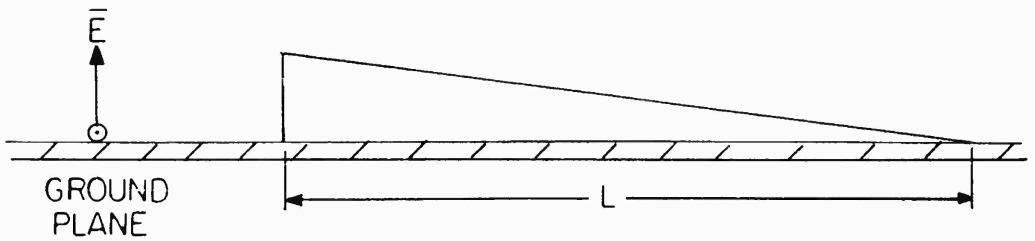

FRONT VIEW

FIG. 2.

$$\sigma = 4\pi R^2 \lim_{R \to \infty} \frac{|S_s|}{|S_i|}$$

where R is the distance between the target and the receiver, S_s is the scattered power flux density, and S_i is the incident power flux density. In other words, the back-scatter cross section of a target is proportional to the square of the back-scattered electric field. To avoid the problem of finding the proportionality constant, we use a sphere, the scattering characteristics of which are well known, as the reference. Since the back-scatter cross section of a sphere has been computed theoretically, all measurements shall be relative to a 4.5 in. perfectly conducting sphere, expressed as the number of decibels above or below that of this sphere.

III. DISCUSSION OF RESULTS

The back-scatter patterns for the 0.619 in. base diameter dielectric cones are shown in Figs. 3, 4, 5, and 6; for the 1 in. cones are shown in Figs. 8, 9, 10, and 11, and for the 1.267 in. cones are shown in Figs. 14, 15, and 16. The 1.267 in. cone corresponding to the relative dielectric constant 10 is not shown because it was damaged beyond repair during the process of machining. For comparison with these dielectric cones, the patterns of the metal cones with base diameters of 0.619 in., 1 in., and 1.267 in. are shown in Figs. 7, 12, and 17, respectively. The circles are calibrated to read the back-scatter cross sections, σ, in decibels relative to that of a 4.5 in. metal sphere.

Repeated measurements of the patterns were taken over a period of days. Each time identical details appeared consistently for each cone. The dissimilarity of the patterns between the dielectric and metal cones even for high dielectric constants is rather surprising; hence, these results repudiate the anticipation that a high degree of resemblance should be observed between the metal and high dielectric constant cones.

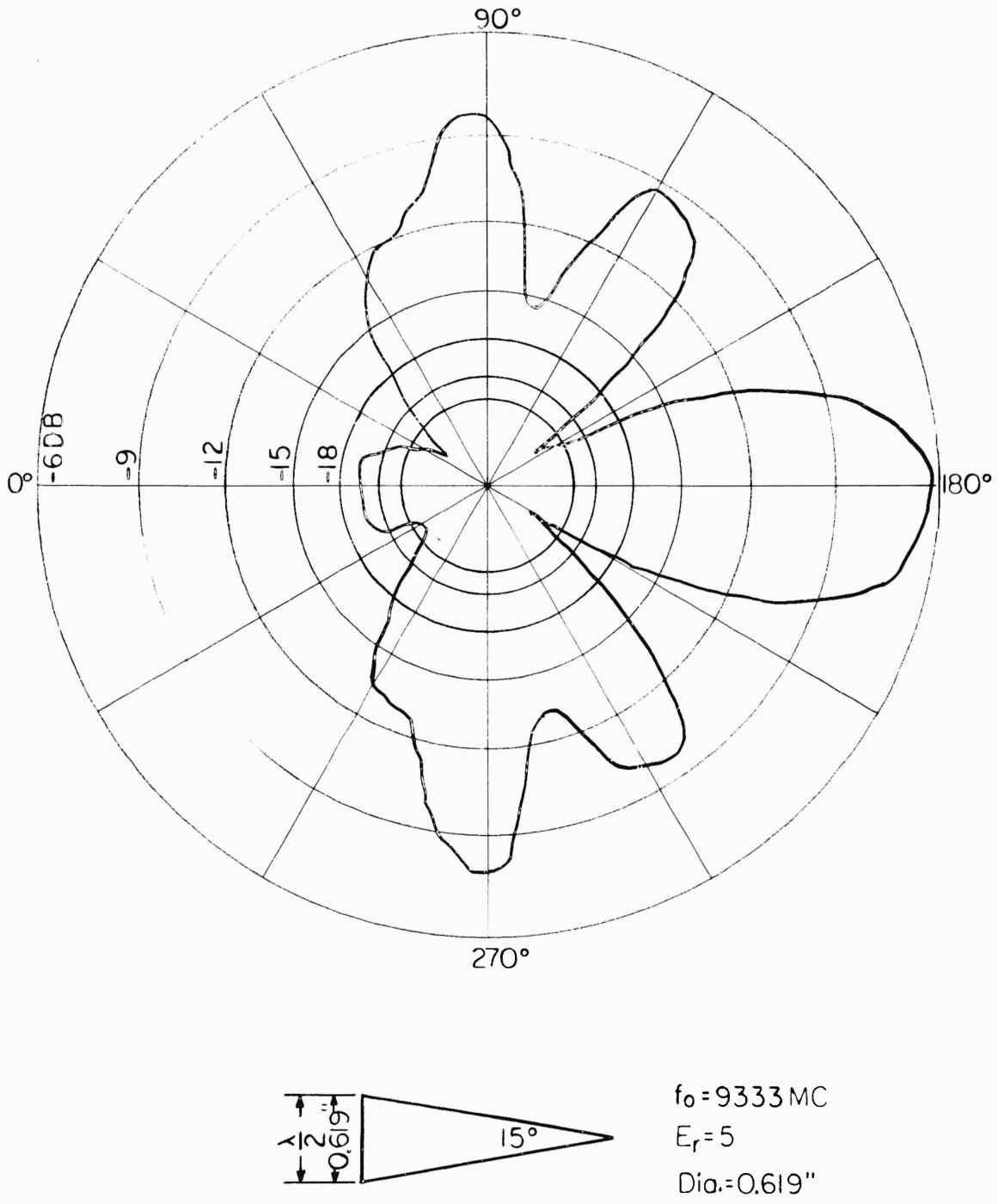

FIG. 3.

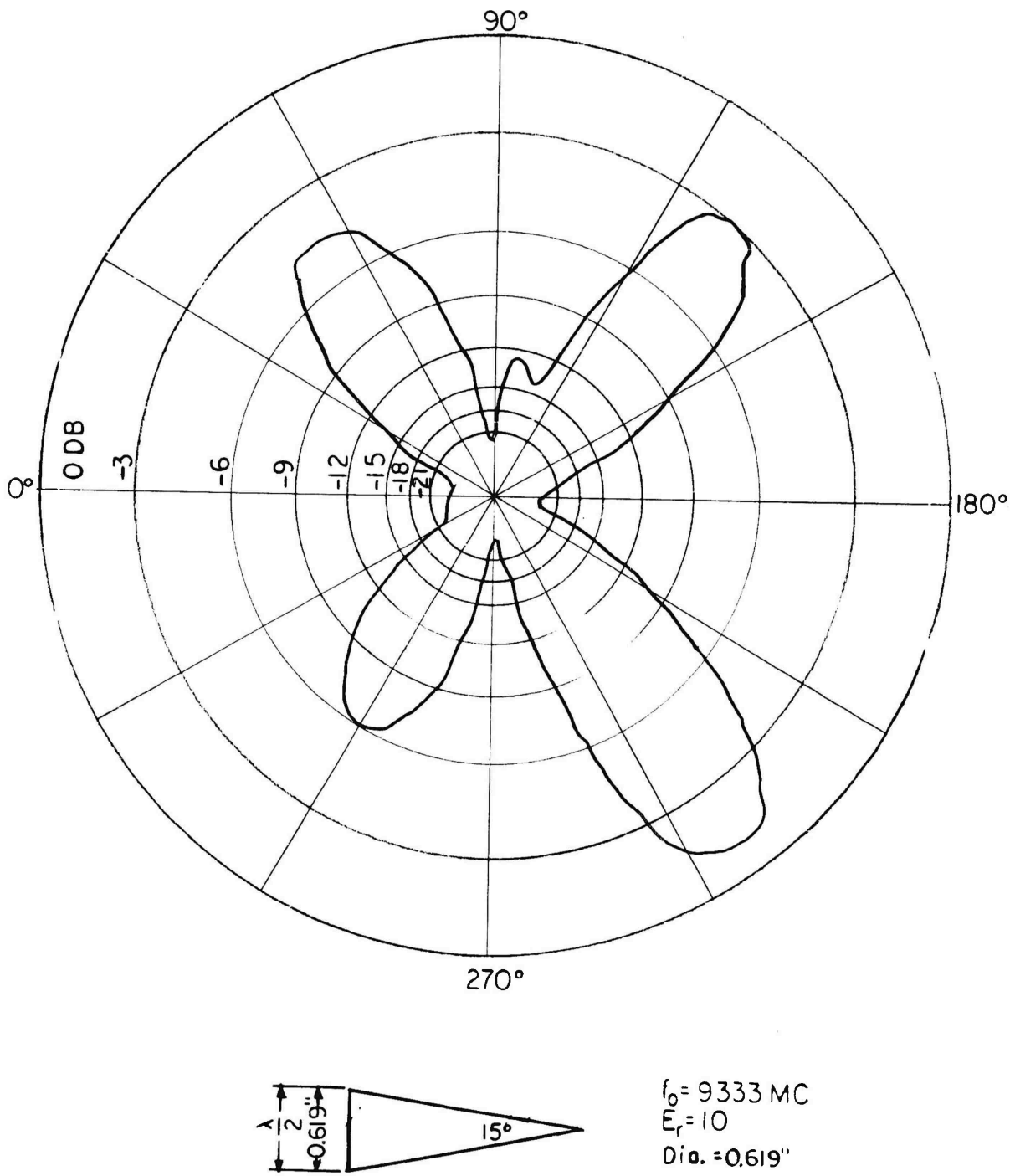
90°
0°
180°
270°
0 DB
-3
-6
-9
-12
-15
-18
-21
λ/2
0.619"
15°
f_0 = 9333 MC
E_r = 10
Dia. = 0.619"

FIG. 4.

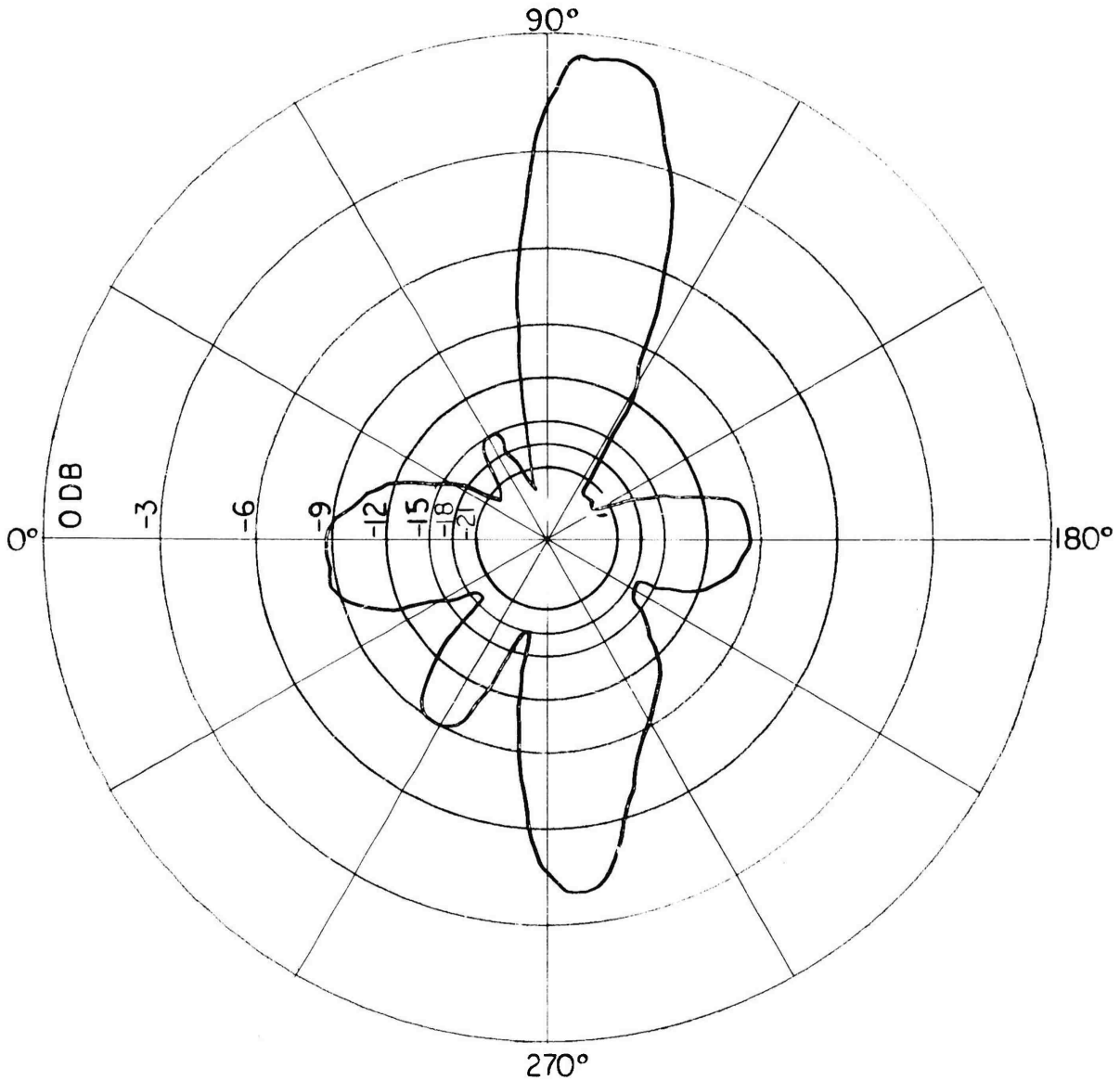

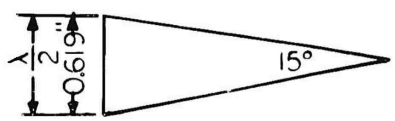

f_o = 9333 Mc
E_r = 15
Dia. = 0.619"

FIG. 5.

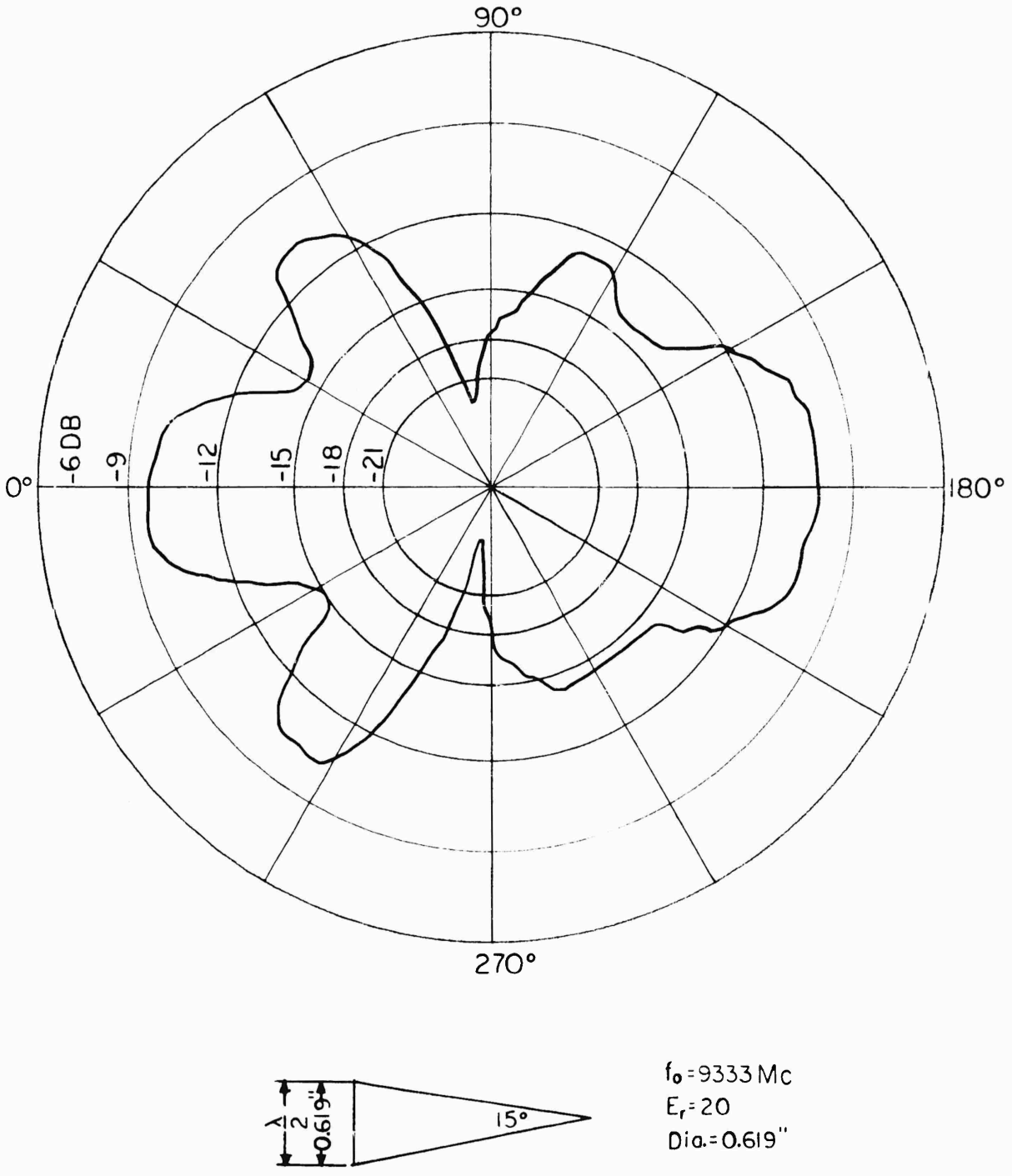

FIG. 6.

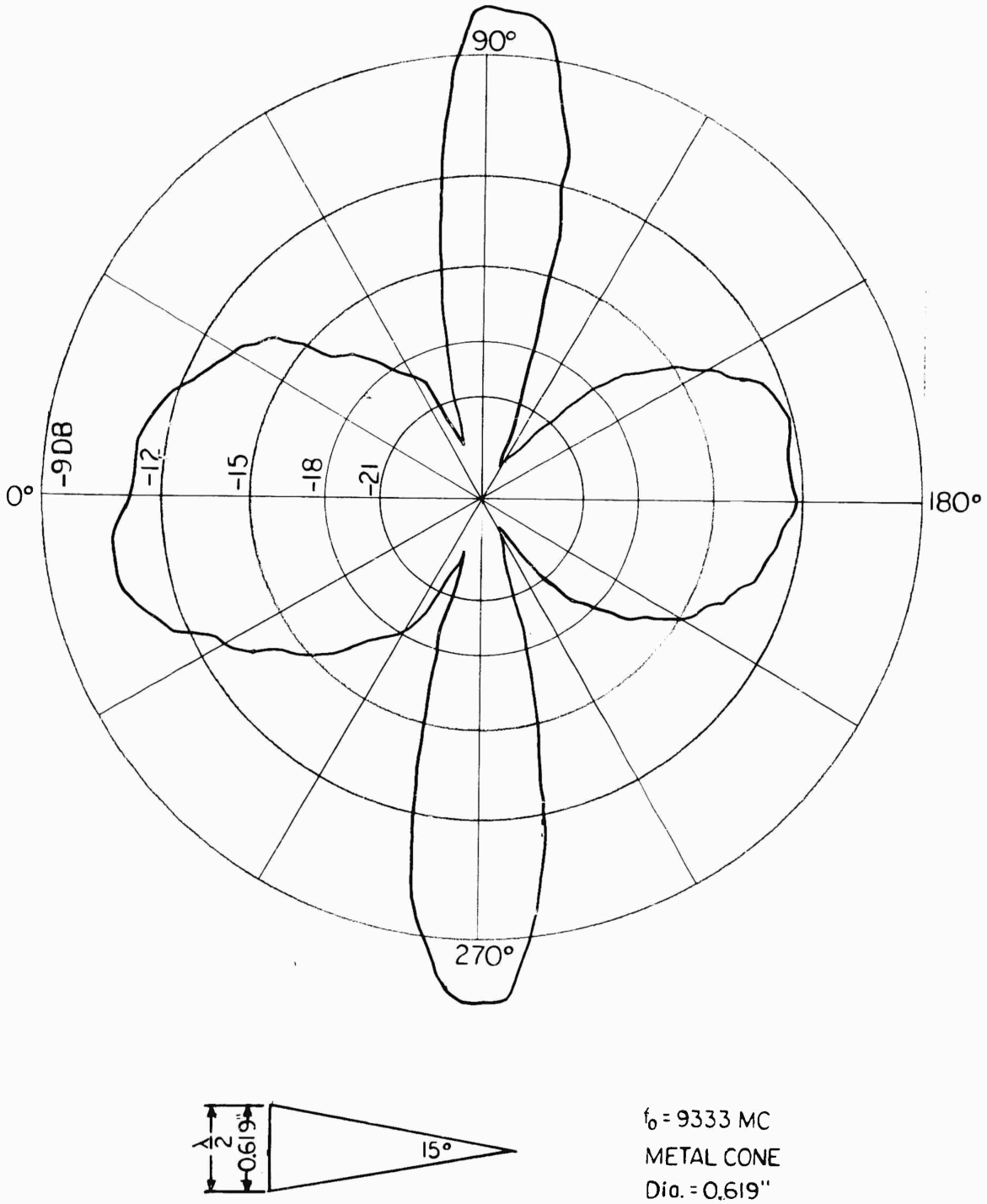
90°
0°
180°
270°
-90dB
-12
-15
-18
-21
λ/2
0.619"
15°
f_0 = 9333 MC
METAL CONE
Dia. = 0.619"

FIG. 7.

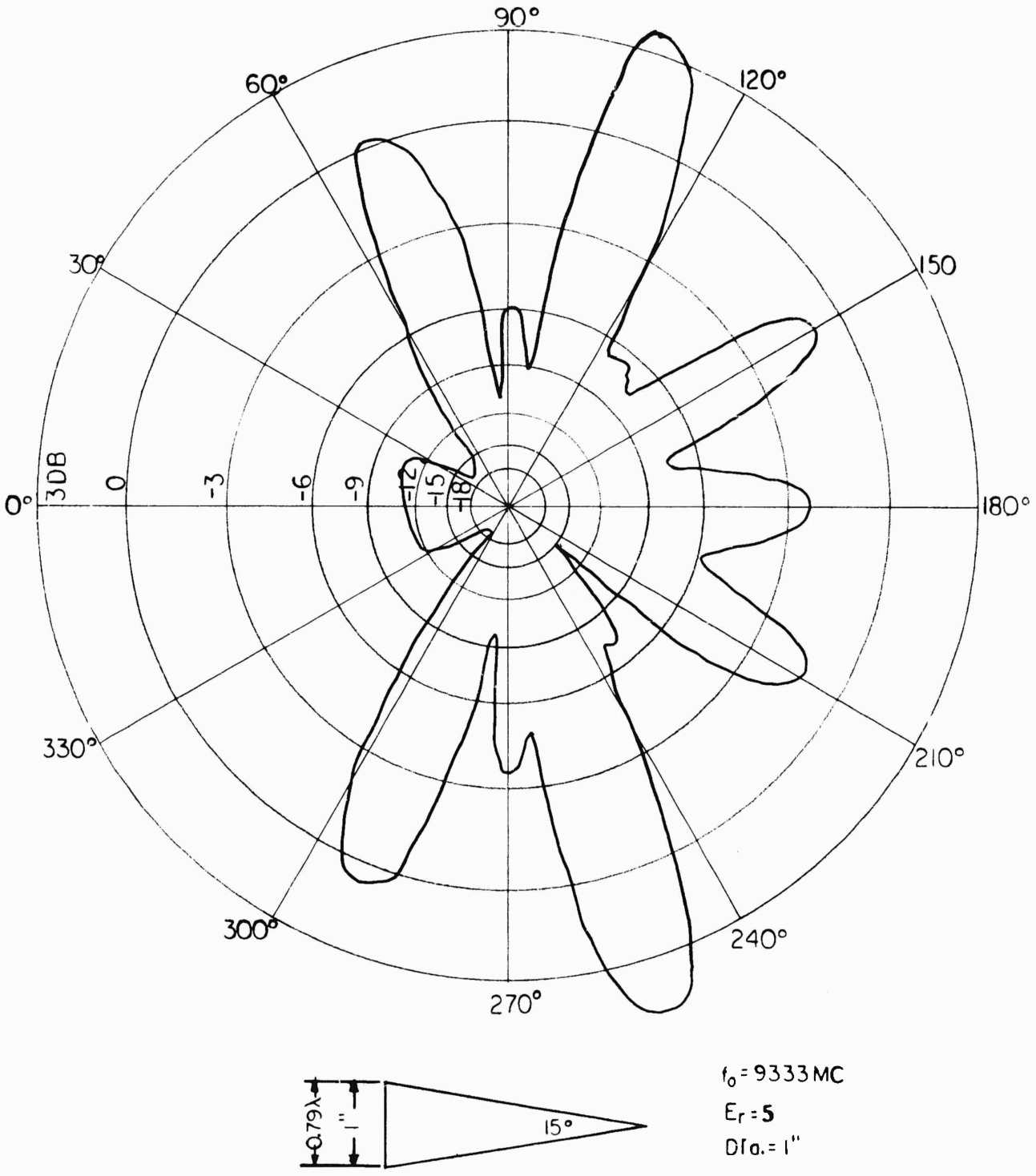
90°
60°
120°
30°
150
0°
180°
330°
210°
300°
240°
270°
3DB
0
-3
-6
-9
-12
-15
-18
0.79λ
1"
15°
f_0 = 9333 MC
E_r = 5
Dia. = 1"

FIG. 8.

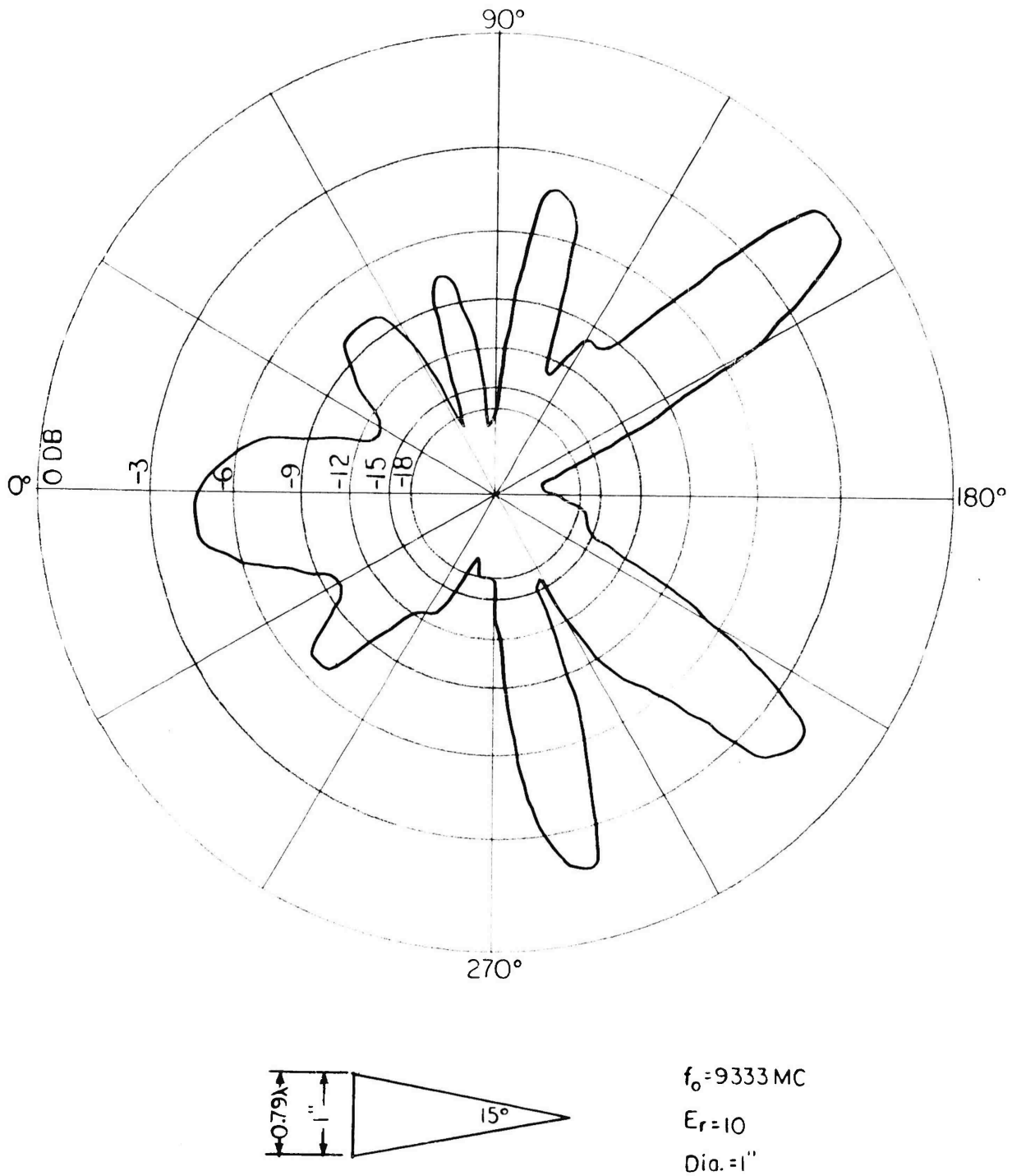

FIG. 9.

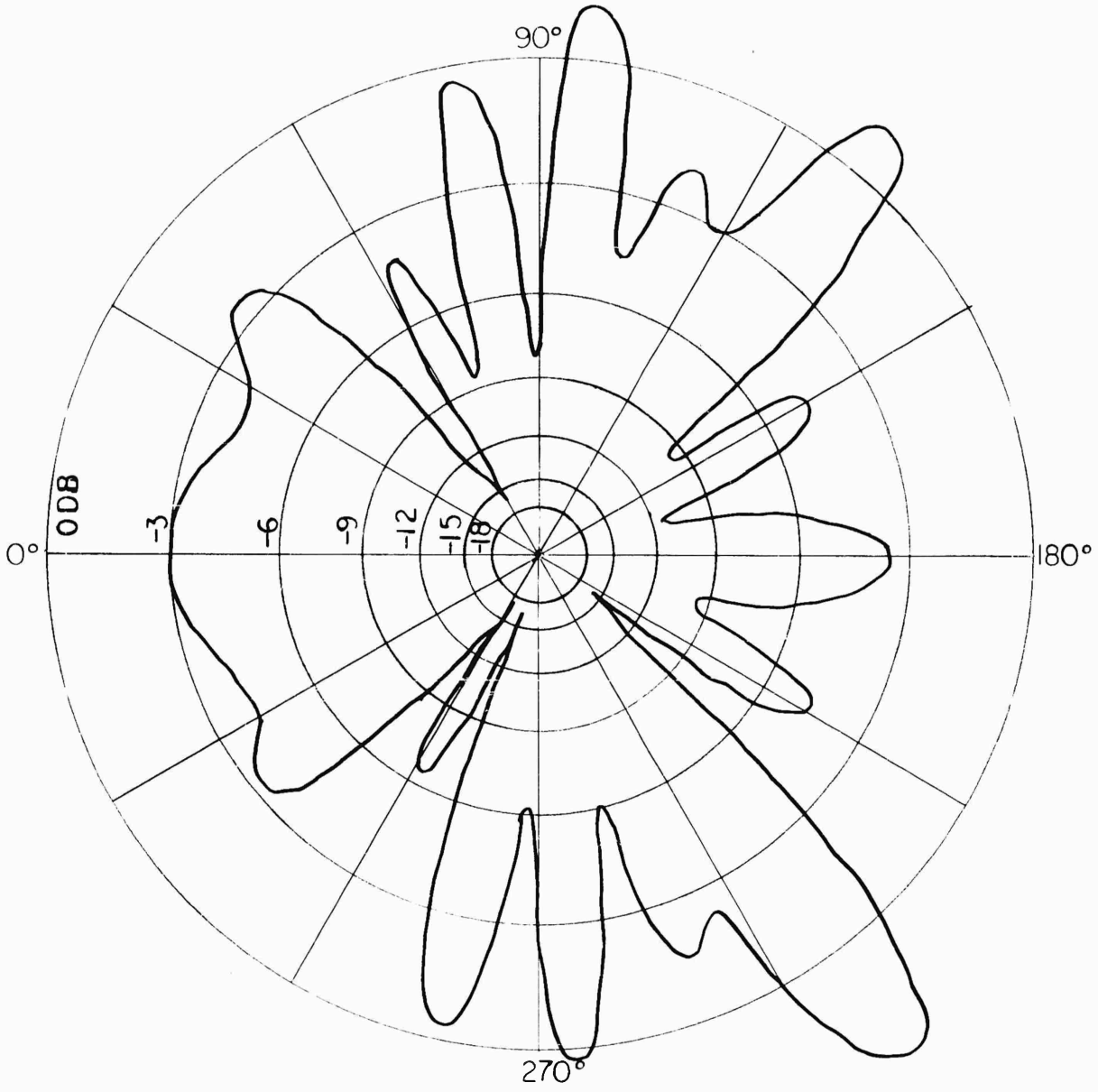

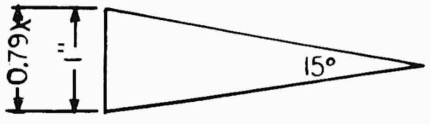

$f_0 = 9333$ MC

$E_r = 15$

Dia. = 1"

FIG. 10.

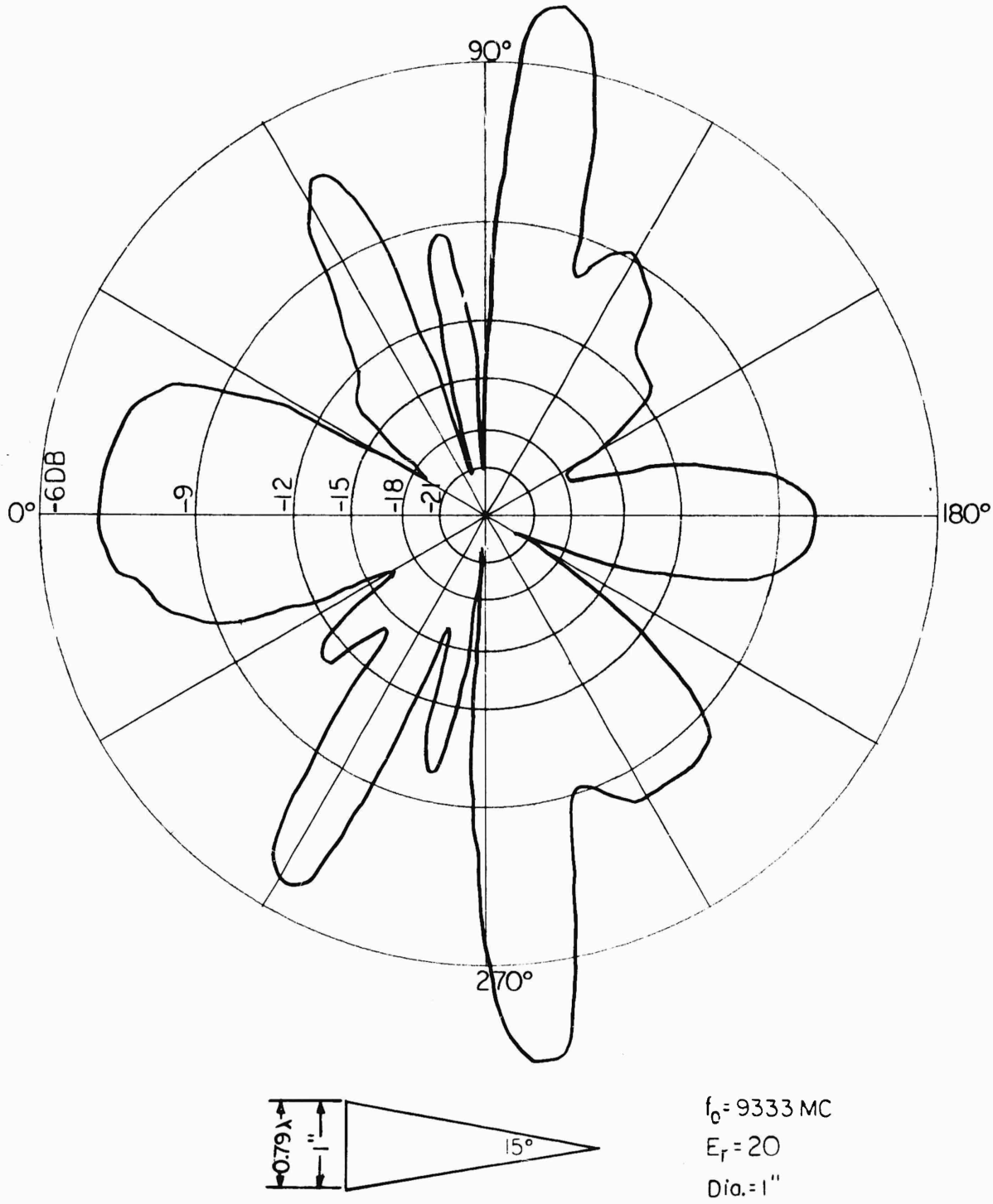

FIG. 11.

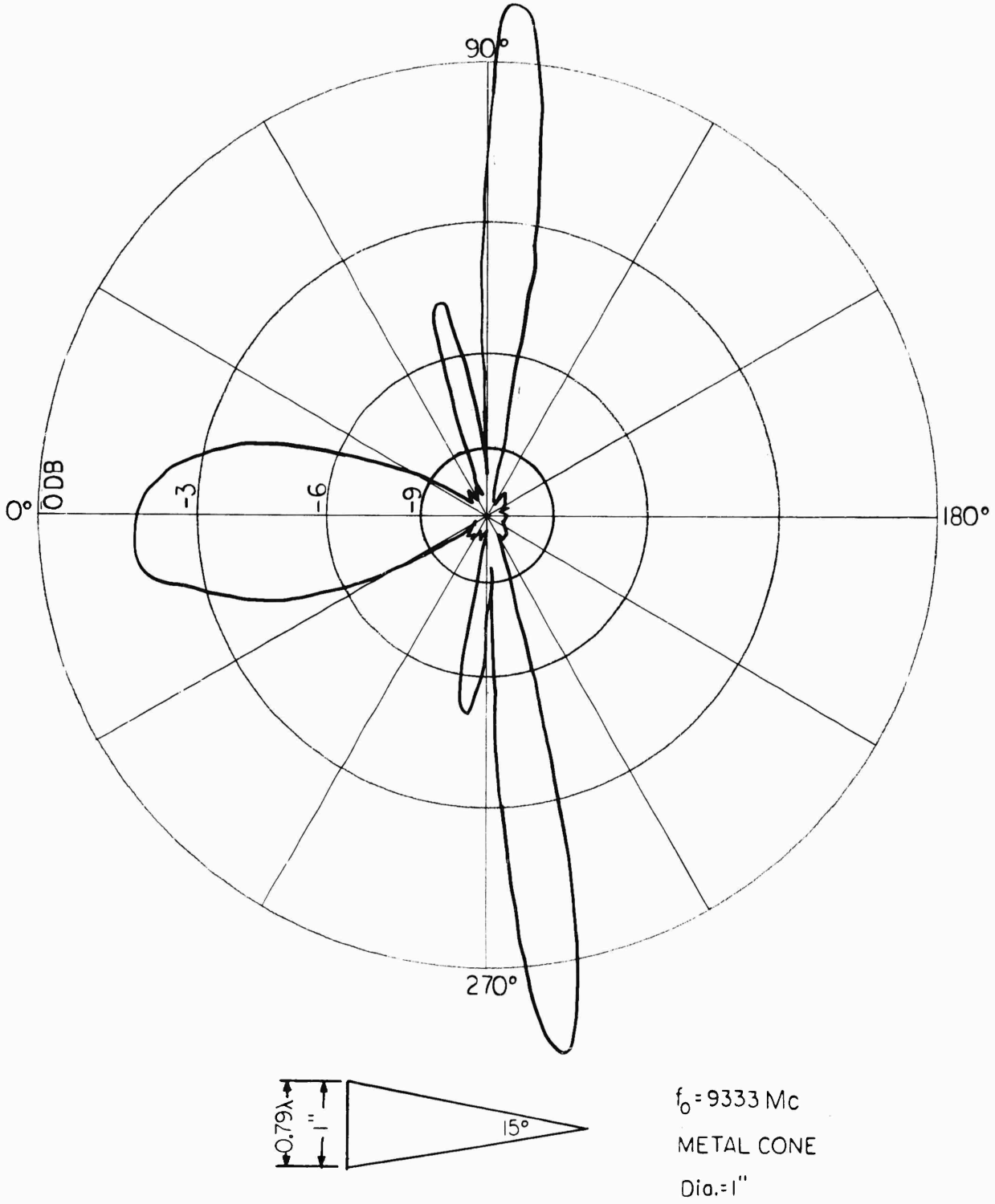

FIG. 12.

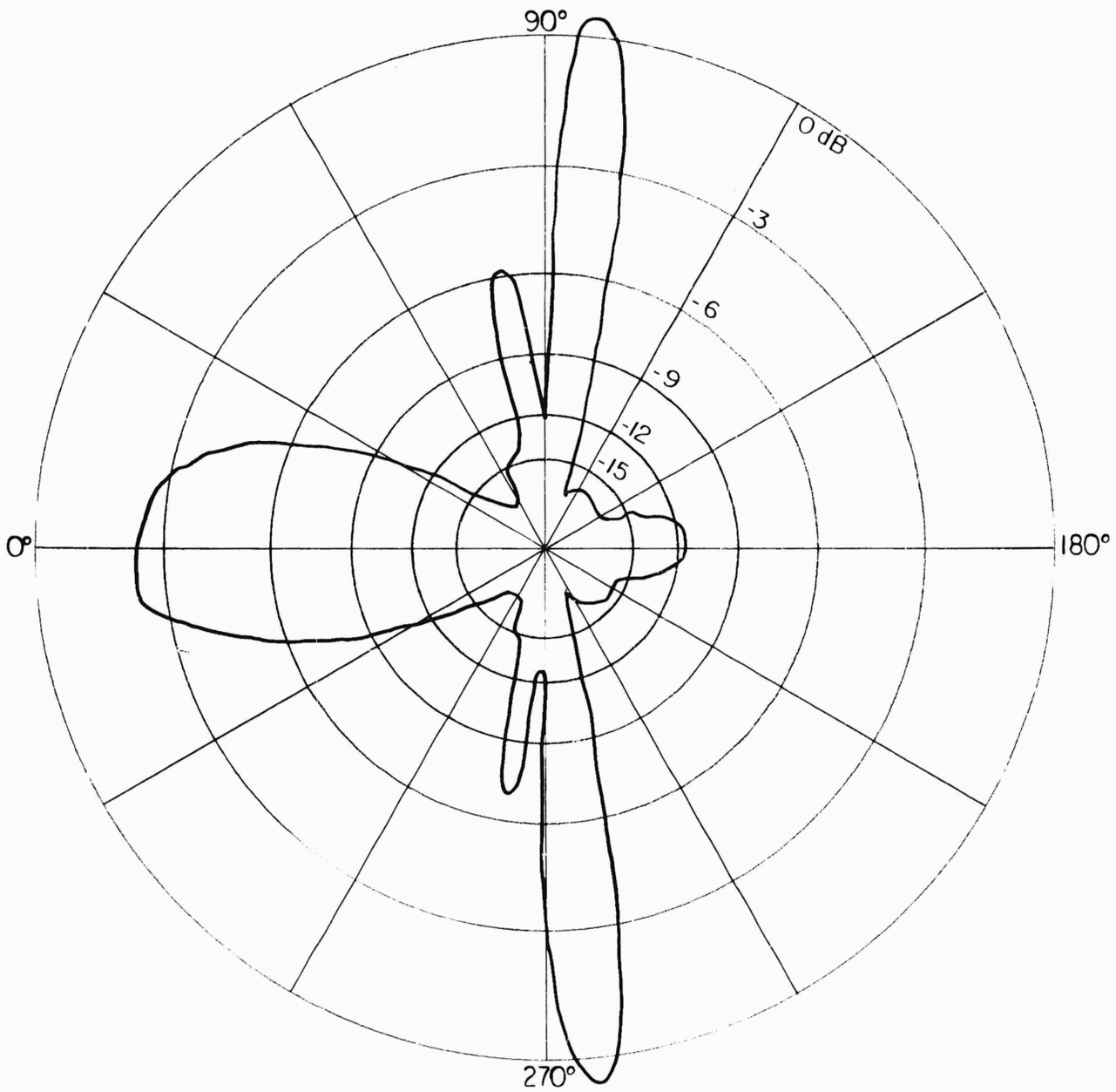
90°
0 dB
-3
-6
-9
-12
-15
0°
180°
270°
15°
0.26λ
f_0 = 9333 MC
LOSSY METAL CONE
Dia. = 1"

FIG. 13.

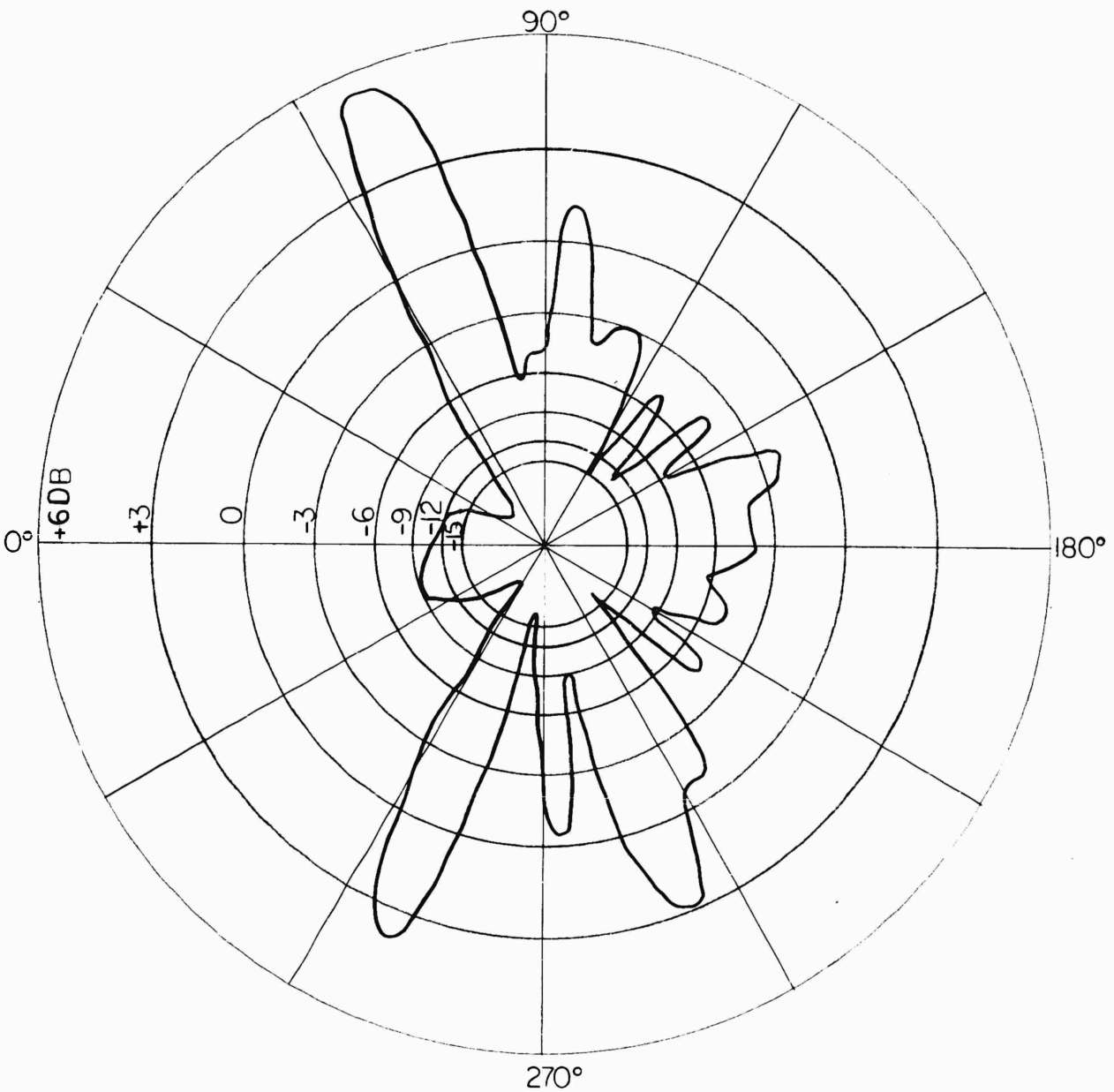

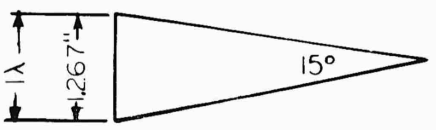

$f_0 = 9333$ MC

$E_r = 5$

Dia. = 1.267"

FIG. 14.

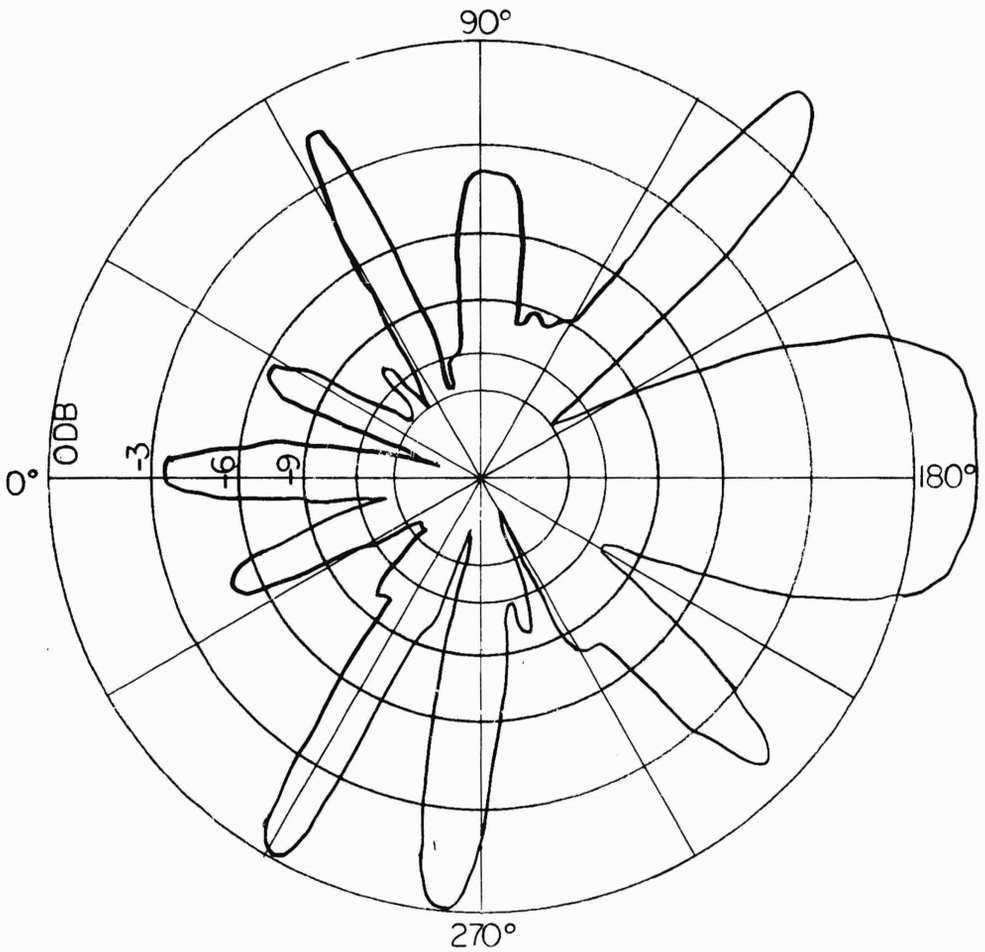

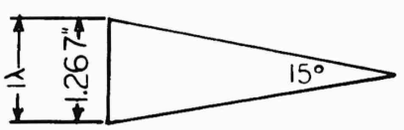

f_o = 9333 MC

E_r = 15

Dia. = 1.267"

FIG. 15.

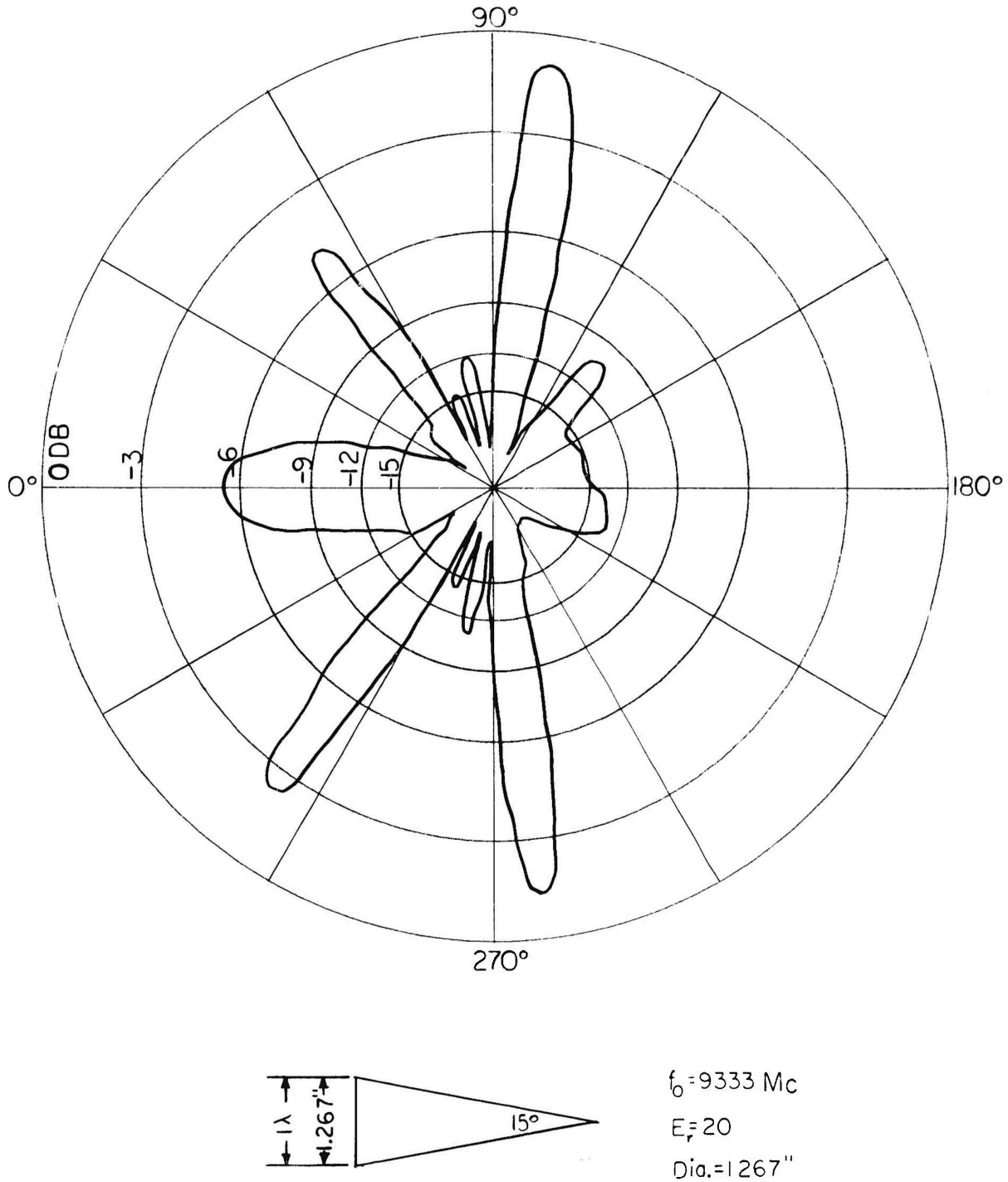

FIG. 16.

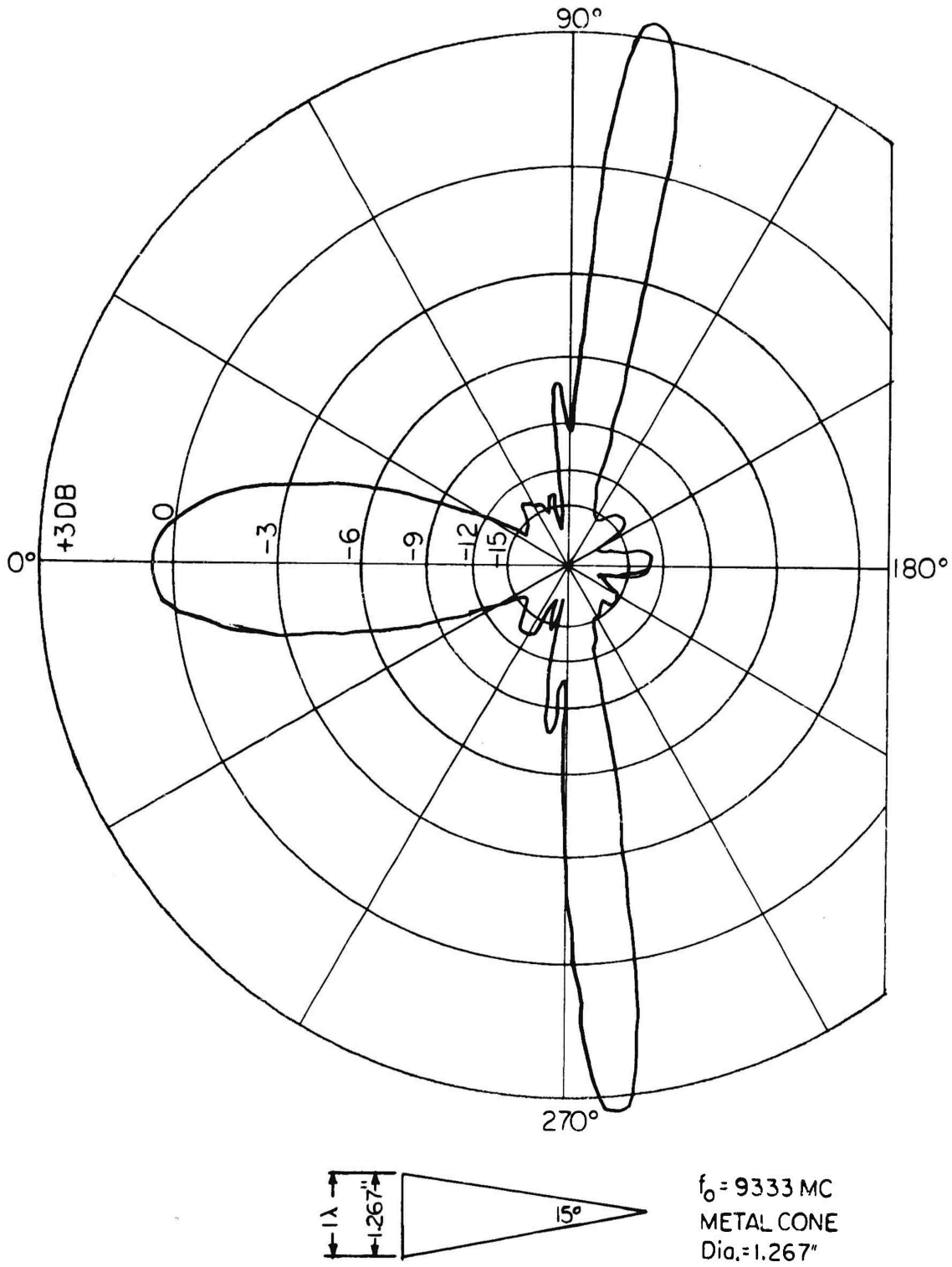
90°
0°
180°
270°
+3DB
0
-3
-6
-9
-12
-15
1λ
1.267"
15°
f_o = 9333 MC
METAL CONE
Dia.=1.267"

FIG. 17.

One of the most distinctive differences between the larger metal and dielectric cones is that the number of lobes appearing in the patterns for the dielectric cones is greater than that in the metal cones, which contain three lobes--the base and two edge lobes by specular reflections. Some of the major lobes, with magnitudes comparable to or even greater than that of the specular reflection from the edge of the metal cones, appear at aspect angles which is not readily perceived intuitively, indicating radiation of a complex nature from induced sources within the cone.

It is interesting to note that for the cones with relative dielectric constant 5 the back-scattered power from the base is very small. For higher dielectric constants the base-on back-scattered power grows progressively larger. This phenomenon may be explained by the following reasons. Since, for an incident plane wave normal to the surface, the magnitude of the reflection coefficient of a slab of dielectric of dielectric constant 5 is 0.382, considerable amount of the incident power will be transmitted inside the dielectric material. This transmitted power undergoes multiple reflections within the dielectric cone, and a portion of this power will be back-scattered. When this reflected power from within the cone comes out the base and combines with the power reflected directly from the base in such a phase that destructive interference occurs, then the total base-on back-scattered power observed will be small. For higher dielectric constant materials, the reflection coefficients are larger and the direct reflection from the base predominates over the reflection from within the cone. Therefore, the base-on back-scattered power increases with increasing dielectric constants.

Another notable difference between the metal and dielectric cones is, in nearly all cases, the surprisingly large reflections from the dielectric cones for the nose-on aspect. Unlike the metal cones which do not allow the waves to penetrate inside the perfect conductors, the dielectric cones have secondary reflections from within the cones which might account for the back-scattered power for the nose-on aspect. Also the imperfections on the surface of the cones may also

contribute to this reflected power.

The only resemblance of the dielectric to the metal cones is that the large specular reflections from the edge at 97.5° begin to appear for large cones of high dielectric constants.

It is observed that the back-scattered power from the cone of dielectric constant 20 is smaller than from the lower dielectric constant cones. This decrease is caused by the higher losses in the former as shown in Table 5. Since all the dielectric cones have losses associated with them, it is of interest to see how the losses affect the pattern of a lossless case. Therefore, a 1 in. metal cone was covered by a coat of lossy material, and the measured pattern shown in Fig. 13 indicates a decrease in return power and the appearance of a small reflected power for the nose-on aspect.

The results obtained by the second type of measurement are shown in Tables 1, 2, and 3. Here the back-scatter cross sections of the base, tip, and major lobes corresponding to those shown in the patterns are measured by the averaging process, which reduces the errors in the pattern measurements. The angles at which the lobe maximums appear in the patterns are verified by rotating the cone slightly away from these angles when the cone is placed at a point other than that of the center of the turntable.

To estimate the accuracy of the results by the averaging method of measurement, a series of measurements by the same method was made on the metal spheres with diameters of 6 in., 4.5 in., and 3 in., the back-scatter cross sections of which have been computed. The results shown in Table 4 indicate that an accuracy better than 0.5 db can be attained by this method.

It is noted that in some cases the patterns lack the complete symmetry. The major cause of this phenomenon is the imperfections on the cones. Any voids on the cones will appear as severe discontinuities. The flatness of the cone is especially a critical factor since good contact between the cone and the ground plane is essential. It is extremely difficult to machine a perfectly smooth cone because of the nature of the dielectric materials. Also any nonuniformity of

TABLE 1. Back-Scatter Cross Sections

CONE DIA. = 0.619 in. = .49λ FREQ. = 9333 Mc

ϵ_r	Aspect Angles Corresponding to Lobe Maximums in Fig. 3 θ	Back-Scatter Cross Sections Relative to a 4.5" sphere $\sigma/\sigma_{4.5"}$
5	(1) 0°--base	-18.48 DB
	(2) 90°	- 8.65
	(3) 122°	- 8.55
	(4) 180°--tip	- 6.05
	θ From Fig. 4	
10	(1) 0°--base	< -18.9 DB
	(2) 53°	- 5.0
	(3) 130°	- 3.4
	(4) 180°--tip	< -18.9
	θ From Fig. 5	
15	(1) 0°--base	-9.1 DB
	(2) 95°	-0.4
	(3) 180°--tip	-9.5
	θ From Fig. 6	
20	(1) 0°--base	- 8.92 DB Metal -11.2 DB
	(2) 50°	-11.12
	(3) 180°--tip	-11.8

TABLE 2. Back-Scatter Cross Sections.

CONE DIA. = 1.0 in. = .79λ FREQ. = 9333 Mc

ϵ_r	Aspect Angles Corresponding to Lobe Maximums in Fig. 8 θ	Back-Scatter Cross Sections Relative to a 4.5" sphere $\sigma/\sigma_{4.5"}$
5	(1) 0^o--base	-14.85 DB
	(2) 68^o	- 1.6
	(3) 108^o	0.05
	(4) 150^o	- 3.15
	(5) 180^o--tip	- 3.45
	θ From Fig. 9	
10	(1) 0^o--base	- 4.7 DB
	(2) 103^o	- 3.1
	(3) 140^o	0.9
	(4) 180^o--tip	< -18.5
	θ From Fig. 10	
15	(1) 0^o--base	-5.15 DB
	(2) 95^o	-0.6
	(3) 130^o	-0.05
	(4) 180^o--tip	-4.5
	θ From Fig. 11	
20	(1) 0^o--base	-10.5 DB
	(2) 62^o	-11.95
	(3) 98^o	- 6.5
	(4) 180^o--tip	- 9.45

TABLE 3. Back-Scatter Cross Sections.

CONE DIA. = 1.267 in. = λ FREQ. = 9333 Mc

ϵ_r	Aspect Angles Corresponding to Lobe Maximums in Fig. 14 θ	Back-Scatter Cross Sections Relative to a 4.5" sphere
5	(1) 0°--base	-10.22 DB
	(2) 66°	5.15
	(3) 94°	1.1
	(4) 180°--tip	- 0.7
	θ From Fig. 15	
15	(1) 0°--base	-4.8 DB
	(2) 130°	-0.35
	(3) 180°--tip	-0.2
	θ From Fig. 16	
20	(1) 0°--base	-5.8 DB Metal +0.1 DB
	(2) 52°	-2.95
	(3) 97.5°	-1.75

TABLE 4. Calibration Data: Cross Sections of Spheres.

FREQ. = 9.333 kMc

	Sphere Dia.	Atten. Read. at $R_0 = 2.6$ meter	Atten. Read. at $R_0 + \lambda/4$	Ave.	$\frac{\sigma}{\sigma_{6'' \text{ sphere}}}$	Computed $\frac{\sigma}{\sigma_{6'' \text{ sphere}}}$
1st Run	6"	22.5 DB	21.1 DB	21.8 DB	0 DB	0 DB
	4.5"	17.8	20.3	19.05	-2.75	-2.46
	3"	15.1	16.2	15.65	-6.15	-6.18
2nd Run	6"	22.0 DB	21.2 DB	21.6 DB	0 DB	
	4.5"	17.7	19.8	18.75	-2.85	
	3"	14.6	16.0	15.3	-6.3	
3rd Run	6"	22.2 DB	20.8 DB	21.5 DB	0 DB	
	4.5"	17.5	19.6	18.55	-2.95	
	3"	14.0	16.1	15.05	-6.45	

TABLE 5. Stycast Hi K Dielectric Materials Manufactured By Emerson And Cuming, Inc.

Electrical Properties.	
Accuracy of Dielectric Constant	0.15 maximum
Dissipation Factor for ϵ_r = 5, 10, 15	below 0.001
for ϵ_r = 20	below 0.01
Volume Resistivity	greater than 10^{14} ohm-cm^3
Dielectric Strength	greater than 500 volts/mil

Physical Properties. Average Values	
Specific Gravity	1.3
Tensile Strength, psi	8,000
Flexural Strength, psi	13,000
Modulus of Elasticity	2×10^5
Coefficient of Linear Expansion	50×10^{-6} cm/cm/$^\circ$C
Water Absorption (% gain in 24 hrs. at 25°C)	0.1

density within the cone will give rise to an unsymmetrical pattern. This point was verified by making the pattern measurements on two carefully machined dielectric cylinders as shown in Fig. 18. Here again the imperfections in fabrication may also enter into the picture to some extent.

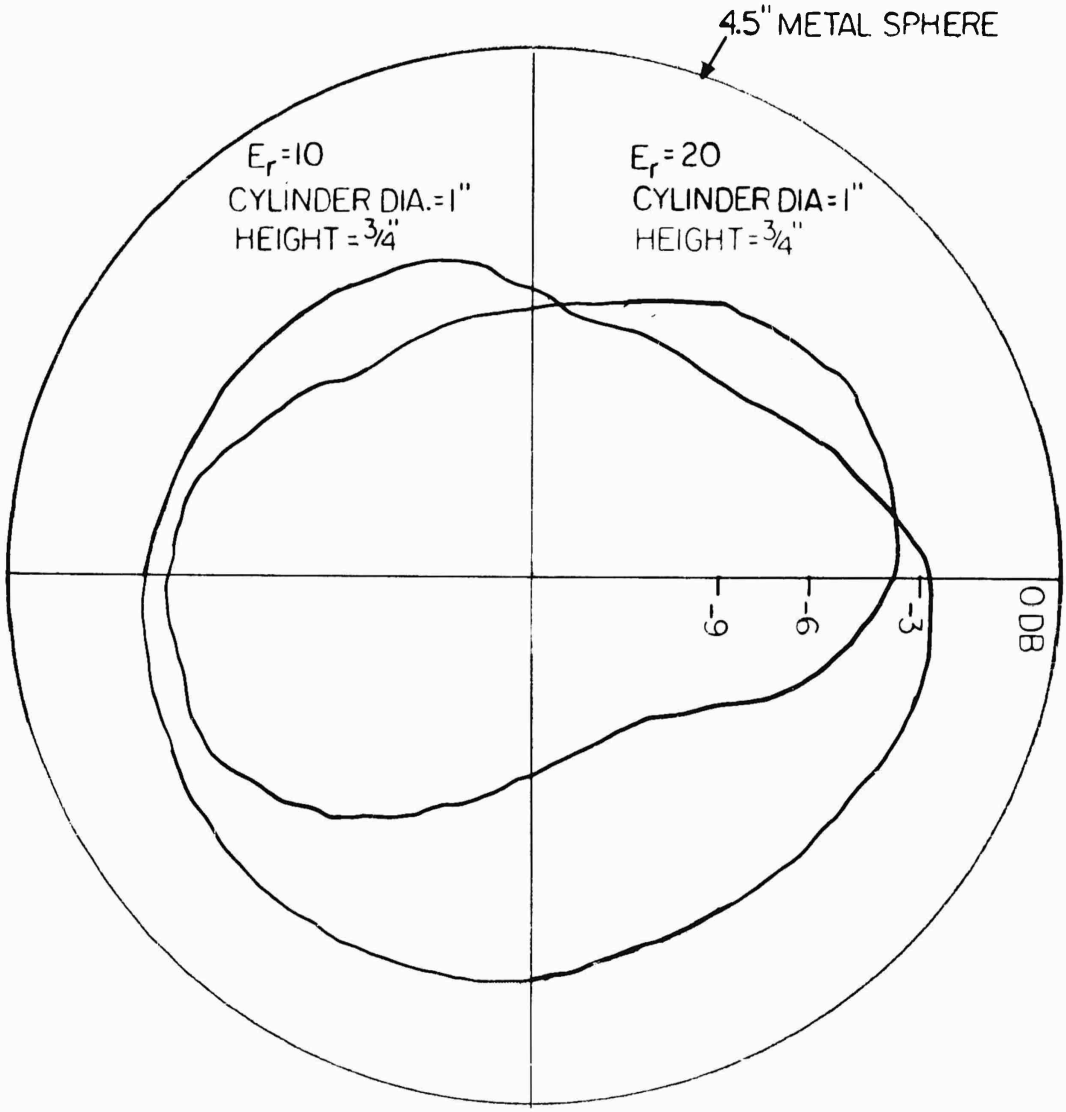
4.5" METAL SPHERE
E_r=10
CYLINDER DIA.=1"
HEIGHT=3/4"
E_r=20
CYLINDER DIA=1"
HEIGHT=3/4"
-9
-6
-3
0DB

FIG. 18.

APPENDIX

TABLE 6. Data: Back-Scatter Cross Sections, σ, at Preselected Aspect Angles.

CONE DIA. = 0.619 in. = $\lambda/2$ FREQ. = 9333 Mc

ϵ_r	θ From Fig. 3	1. Attenuator Reading for Target at R = 2.6 meter	2. Attenuator Reading at R + $\lambda/4$	Ave. of 1 and 2
5	(1) 0°--base	0.74 DB	0.1 DB	0.42 DB
	(2) 90°	11	9.5	10.25
	(3) 122°	10.0	10.7	10.35
	(4) 180°--tip	13.0	12.7	12.85
	4.5" metal sphere	17.9	19.9	18.9
	θ From Fig. 4			
10	(1) 0°--base	<0 DB	<0 DB	<0 DB
	(2) 53°	14.1	13.7	13.9
	(3) 130°	15.4	15.6	15.5
	(4) 180°--tip	<0	<0	<0
	4.5" metal sphere	17.8	20.0	18.9
	θ From Fig. 5			
15	(1) 0°--base	8.3 DB	11.2 DB	9.75 DB
	(2) 95°	18.5	18.4	18.45
	(3) 180°--tip	10.1	8.6	9.35
	4.5" metal sphere	18.1	19.6	18.85
	θ From Fig. 6			
20	(1) 0°--base	9.15 DB	10.2 DB	9.68 DB
	(2) 50°	6.7	8.25	7.48
	(3) 180°--tip	7.3	6.3	6.8
	4.5" metal sphere	17.7	19.5	18.6

TABLE 7. Data: Back-Scatter Cross Sections, σ, at Preselected Aspect Angles.

CONE DIA. = 1.0 in. = 0.79λ FREQ. = 9333 Mc

ϵ_r	θ From Fig. 8	1. Attenuator Reading for Target at R = 2.6 meter	2. Attenuator Reading at R + λ/4	Ave. of 1 and 2
5	(1) 0°--base	2.4 DB	5.9 DB	4.15 DB
	(2) 68°	17.3	17.5	17.4
	(3) 108°	19.8	18.3	19.05
	(4) 150°	15.7	16.0	15.85
	(5) 180°--tip	15.3	15.8	15.55
	4.5" sphere	18.0	20	19
	θ From Fig. 9			
10	(1) 0°	13.8 DB	13.8 DB	13.8 DB
	(2) 103°	15.5	15.3	15.4
	(3) 140°	17.8	17.4	17.6
	(4) 180°	0	0	0
	4.5" sphere	17.4	19.5	18.5
	θ From Fig. 10			
15	(1) 0°	13.9 DB	13.8 DB	13.85 DB
	(2) 95°	18.1	18.7	18.4
	(3) 130°	19.5	18.4	18.95
	(4) 180°	13.8	15.2	14.5
	4.5" sphere	18	20	19
	θ From Fig. 11			
20	(1) 0°	8.1 DB	9.7 DB	8.9 DB
	(2) 62°	7.7	7.2	7.45
	(3) 98°	13.1	12.7	12.9
	(4) 180°	9.6	10.3	9.95
	4.5" sphere	18.8	19.9	19.4

TABLE 8. Data: Back-Scatter Cross Sections, σ, at Preselected Aspect Angles.

CONE DIA. = 1.237 in. = λ FREQ. = 9333 Mc

ϵ_r	θ From Fig. 14	1. Attenuator Reading for Target at R = 2.6 meter	2. Attenuator Reading at R + $\lambda/4$	Ave. of 1 and 2
5	(1) 0°	9.25 DB	7.5 DB	8.38 DB
	(2) 66°	23.5	24.0	23.75
	(3) 94°	20.3	19.1	19.7
	(4) 180°	18.3	17.5	17.9
	4.5" sphere	17.7	19.5	18.6
	θ From Fig. 15			
15	(1) 0°	14.3 DB	14.1 DB	14.2 DB
	(2) 130°	18.9	18.4	18.65
	(3) 180°	19.1	18.5	18.8
	4.5" sphere	18.0	20.0	19.0
	θ From Fig. 16			
20	(1) 0°	13.4 DB	13.0 DB	13.2 DB
	(2) 52°	15.2	16.9	16.05
	(3) 97.5°	18.1	16.4	17.25
	(4) 180°			
	4.5" sphere	18.0	20.0	19.0

TABLE 7. Data: Back-Scatter Cross Sections, σ, at Preselected Aspect Angles.

CONE DIA. = 1.0 in. = 0.79λ FREQ. = 9333 Mc

ϵ_r	θ From Fig. 8	1. Attenuator Reading for Target at R = 2.6 meter	2. Attenuator Reading at R + $\lambda/4$	Ave. of 1 and 2
5	(1) 0°--base	2.4 DB	5.9 DB	4.15 DB
	(2) 68°	17.3	17.5	17.4
	(3) 108°	19.8	18.3	19.05
	(4) 150°	15.7	16.0	15.85
	(5) 180°--tip	15.3	15.8	15.55
	4.5" sphere	18.0	20	19
	θ From Fig. 9			
10	(1) 0°	13.8 DB	13.8 DB	13.8 DB
	(2) 103°	15.5	15.3	15.4
	(3) 140°	17.8	17.4	17.6
	(4) 180°	0	0	0
	4.5" sphere	17.4	19.5	18.5
	θ From Fig. 10			
15	(1) 0°	13.9 DB	13.8 DB	13.85 DB
	(2) 95°	18.1	18.7	18.4
	(3) 130°	19.5	18.4	18.95
	(4) 180°	13.8	15.2	14.5
	4.5" sphere	18	20	19
	θ From Fig. 11			
20	(1) 0°	8.1 DB	9.7 DB	8.9 DB
	(2) 62°	7.7	7.2	7.45
	(3) 98°	13.1	12.7	12.9
	(4) 180°	9.6	10.3	9.95
	4.5" sphere	18.8	19.9	19.4

TABLE 8. Data: Back-Scatter Cross Sections, σ, at Preselected Aspect Angles.

CONE DIA. = 1.237 in. = λ FREQ. = 9333 Mc

ϵ_r	ϕ From Fig. 14	1. Attenuator Reading for Target at R = 2.6 meter	2. Attenuator Reading at R + λ/4	Ave. of 1 and 2
5	(1) 0°	9.25 DB	7.5 DB	8.38 DB
	(2) 66°	23.5	24.0	23.75
	(3) 94°	20.3	19.1	19.7
	(4) 180°	18.3	17.5	17.9
	4.5" sphere	17.7	19.5	18.6
	θ From Fig. 15			
15	(1) 0°	14.3 DB	14.1 DB	14.2 DB
	(2) 130°	18.9	18.4	18.65
	(3) 180°	19.1	18.5	18.8
	4.5" sphere	18.0	20.0	19.0
	θ From Fig. 16			
20	(1) 0°	13.4 DB	13.0 DB	13.2 DB
	(2) 52°	15.2	16.9	16.05
	(3) 97.5°	18.1	16.4	17.25
	(4) 180°			
	4.5" sphere	18.0	20.0	19.0

REFERENCES

1. K. M. Siegel, et al., "Comparison between Theory and Experiment of the Cross Section of a Cone," Willow Run Research Center, Engineering Research Institute, University of Michigan, February 1953.

2. J. W. Crispin, Jr., R. E. Goodrich, and K. M. Siegel, "A Theoretical Method for the Calculation of the Radar Cross Sections of Aircraft and Missiles," The University of Michigan, College of Engineering, Dept. of Electrical Engineering, July 1959.

3. J. Honda, S. Silver, and F. D. Clapp, "Scattering of Microwaves by Figures of Revolution," Electronics Research Laboratory, University of California, Series No. 60, Issue No. 232, March 16, 1959.

4. J. Honda, M. S. Thesis, University of California, Berkeley, 1959.

5. A. Olte, "Precision Measurement of Scattering from Figures of Revolution," Ph. D. Thesis, University of California, Berkeley, 1959.

6. G. August, D. J. Angelakos, "Back-Scattering from Cones," Electronics Research Laboratory, University of California, Series No. 60, Issue No. 252, September 22, 1959.